Biogeosciences

Ecosystem responses to elevated CO_2 using airborne remote sensing at Mammoth Mountain, California

Kerry Cawse-Nicholson[1], Joshua B. Fisher[1], Caroline A. Famiglietti[1], Amy Braverman[1], Florian M. Schwandner[1,2],
Jennifer L. Lewicki[3], Philip A. Townsend[4], David S. Schimel[1], Ryan Pavlick[1], Kathryn J. Bormann[1], Antonio Ferraz[1],
Emily L. Kang[5], Pulong Ma[5], Robert R. Bogue[1], Thomas Youmans[1], and David C. Pieri[1]

[1]Jet Propulsion Laboratory, California Institute of Technology, Pasadena, CA, USA
[2]Joint Institute for Regional Earth System Science and Engineering, University of California Los Angeles,
Los Angeles, CA, USA
[3]United States Geological Survey, Menlo Park, CA, USA
[4]University of Wisconsin-Madison, Madison, WI, USA
[5]University of Cincinnati, Cincinnati, OH, USA

Correspondence: Kerry Cawse-Nicholson (kcawseni@jpl.nasa.gov)

Abstract. We present an exploratory study examining the use of airborne remote-sensing observations to detect ecological responses to elevated CO_2 emissions from active volcanic systems. To evaluate these ecosystem responses, existing spectroscopic, thermal, and lidar data acquired over forest ecosystems on Mammoth Mountain volcano, California, were exploited, along with in situ measurements of persistent volcanic soil CO_2 fluxes. The elevated CO_2 response was used to statistically model ecosystem structure, composition, and function, evaluated via data products including biomass, plant foliar traits and vegetation indices, and evapotranspiration (ET). Using regression ensemble models, we found that soil CO_2 flux was a significant predictor for ecological variables, including canopy greenness (normalized vegetation difference index, NDVI), canopy nitrogen, ET, and biomass. With increasing CO_2, we found a decrease in ET and an increase in canopy nitrogen, both consistent with theory, suggesting more water- and nutrient-use-efficient canopies. However, we also observed a decrease in NDVI with increasing CO_2 (a mean NDVI of 0.27 at $200\,\mathrm{g\,m^{-2}\,d^{-1}}$ CO_2 reduced to a mean NDVI of 0.10 at $800\,\mathrm{g\,m^{-2}\,d^{-1}}$ CO_2). This is inconsistent with theory though consistent with increased efficiency of fewer leaves. We found a decrease in aboveground biomass with increasing CO_2, also inconsistent with theory, but we did also find a decrease in biomass variance, pointing to a long-term homogenization of structure

with elevated CO_2. Additionally, the relationships between ecological variables changed with elevated CO_2, suggesting a shift in coupling/decoupling among ecosystem structure, composition, and function synergies. For example, ET and biomass were significantly correlated for areas without elevated CO_2 flux but decoupled with elevated CO_2 flux. This study demonstrates that (a) volcanic systems show great potential as a means to study the properties of ecosystems and their responses to elevated CO_2 emissions and (b) these ecosystem responses are measurable using a suite of airborne remotely sensed data.

---

1 Introduction

Terrestrial ecosystems have consistently taken up carbon over the past century, in excess or balancing losses due to deforestation and land use change, and this sink has grown with time (Le Quéré et al., 2016; Schimel et al., 2015). Much debate, however, has centred on the drivers of this uptake. Suggested mechanisms include nitrogen deposition (Peterson and Melillo, 1985), land use (Schimel, 1995), and the di-

rect effects of carbon dioxide on plant growth (Norby et al., 2016). The last, which proposes that increased atmospheric CO$_2$ yields increased photosynthetic rates, is both the most probable and the most controversial. Although a multitude of experiments have shown positive photosynthetic responses to increased CO$_2$ consistent with the observed growth in the terrestrial sink (Drake et al., 1997), many ecologists have argued that plant growth in intact ecosystems is limited by water, light, or nutrients rather than CO$_2$ (Körner, 2006; McGuire et al., 1995).

The Free-Air Carbon dioxide Enrichment (FACE) experiments, introduced in the 1990s, allow for CO$_2$ fertilization of intact ecosystems by creating controlled fumigation conditions without the use of a growth chamber (Lewin et al., 1994). The FACE studies have been invaluable to our understanding of the CO$_2$ effect, which contributes to the largest uncertainties in projections of Earth's climate. These studies have shown some consistent responses indicative of enhanced growth (Norby et al., 2016), as well as other physiological, morphological, and ecosystem consequences, but also suffer from several structural limitations. Perhaps most notably, only short-term study periods are feasible, and it is difficult to measure slower processes like plant acclimation, shifts in species dominance induced by CO$_2$, or other long-term mechanisms mediated by changes to soil organic matter and nutrients. This is where the long-term localized emissions of volcanic CO$_2$ can play a game-changing role in how to assess the long-term CO$_2$ effect on ecosystems.

As a result of limited empirical evidence for the strength of CO$_2$ fertilization effects, global carbon cycle models disagree about the significance of their associated impacts. Some models show very large CO$_2$ effects, while others indicate a smaller or saturating effect (Kolby Smith et al., 2015). Because future predicted fossil carbon uptake is highly dependent on the strength of the simulated CO$_2$ fertilization, any constraints on the long-term effect of elevated CO$_2$ on ecosystems would be valuable in reducing uncertainty in coupled carbon–climate models (Friedlingstein et al., 2014).

Persistent diffuse volcanic CO$_2$ emissions through soils result from the degassing of magma beneath volcanoes and offer a continuous natural experiment to study vegetation responses to elevated CO$_2$ that is expansive in both space and time. These surface discharges yield broad atmospheric enhancements that transport CO$_2$ downwind (Kerrick, 2001), resulting in swaths of variably affected plants whose periods of exposure can be over hundreds of years (Cook et al., 2001). Because volcanic CO$_2$ emissions are a vital part of the global carbon cycle (Mason et al., 2017; Schwandner et al., 2017) and have been monitored worldwide for decades (Boudoire et al., 2017; Camarda et al., 2012; Perez et al., 2011; Gerlach, 1991), the rate and spatial distribution of these fluxes are well-understood due to an abundance of field surveys in many volcanic systems (e.g. Lewicki et al., 2014; Giammanco et al., 2007; Cardellini et al., 2003; Werner and Brantley, 2003; Hernández et al., 1998). The "kill zone" is
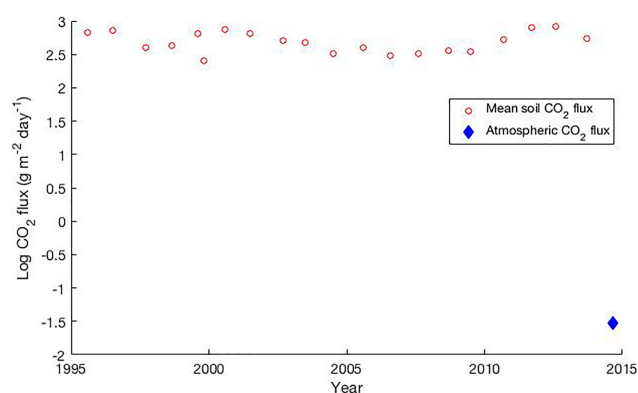
Figure 1. The USGS has measured elevated soil CO$_2$ flux at Horseshoe Lake for the past 2 decades (Werner et al., 2014). These values are consistently higher than the atmospheric CO$_2$ measured by USGS California Volcano Observatory eddy covariance station at Horseshoe Lake at the time of the AVIRIS overpass on 21 October 2014.

the exact location where CO$_2$ is emitted through the soil – a property of the soil being altered by the emission. Although the spatial distributions of CO$_2$ emissions within tree-kill areas have been well mapped (List et al., 2005; Werner and Brantley, 2003; Pickles et al., 2001, and others), linking CO$_2$ measurements to vegetation responses along a spatially diffuse CO$_2$ degassing continuum (outside of the tree-kill zone) is a natural yet underutilized opportunity for studying the effects of elevated CO$_2$ on plants (Schwandner et al., 2004). Furthermore, many CO$_2$ emissions in volcanic systems have been ongoing for decades or centuries, thus allowing for the observation of equilibrium, long-term ecosystem responses after transient and acclimational responses have passed.

While FACE experiments may demonstrate ecological responses to increased CO$_2$ at the outset of elevation, studies in volcanic areas can do the same on super-century scales. However, because volcanic emissions can affect entire landscapes differentially depending on the flow dynamics of the gas, they require new and innovative techniques for analysis. Remote-sensing observations allow for detailed measurements across a wide spatial extent that can be used to analyse ecological indicators of CO$_2$ effects.

Here, we present an exploratory study examining the use of airborne remote-sensing data to detect ecological responses to elevated volcanic CO$_2$ emissions. It is a fundamental principal of volcanology that all active volcanoes emit CO$_2$ continuously during their entire life cycle. We leveraged existing data over Mammoth Mountain, California – a much-studied volcano that has been passively emitting CO$_2$ at high concentrations through faults and fissures on its flanks. The emissions have been measured systematically since a large earthquake swarm in 1989, and their variability has been well documented by repeated CO$_2$ efflux mapping (Lewicki et al., 2014b; Werner et al., 2014; Farrar et al., 1995). Figure

1 shows that the elevated soil CO$_2$ fluxes, measured by the USGS over a span of 2 decades, far exceed the atmospheric CO$_2$ measured by a flux tower at the same site.

We developed a statistical framework for examining the relationships between field measurements of soil CO$_2$ emissions into the air below the forest canopy and a suite of remotely sensed ecological variables. In this investigation, we aim to (i) evaluate the viability of using a passively degassing volcanic system to study the properties of ecosystems, (ii) assess the detectability of ecological responses to elevated soil CO$_2$ emissions via airborne data alone, and (iii) present key lessons enabling future studies to extend our framework to other biomes. This methodology can be applied to any site that is exposed to elevated CO$_2$.

2 Methods

2.1 Data

Airborne remote-sensing data from multiple sources have been acquired over Mammoth Mountain, California, USA, providing a substantial means to assess ecosystem structure (products derived from lidar, such as canopy height and biomass), composition (products derived from spectral data, such as vegetation indices and plant foliar traits), and function (data products derived from thermal data, such as evapotranspiration). Figure 2 illustrates several of the different products used in this study, highlighting the diversity of data sources and spatial resolutions.

Mammoth Mountain is an upper montane forest ecosystem, characterized by abundant *Pinus contorta* (lodgepole pine) and also by mature stands of *Abies magnifica* (red fir), *Pinus jeffreyi* (Jeffrey pine), *Pinus albicaulis* (whitebark pine), and *Juniperus occidentalis* (western juniper) (Potter, 1998). The elevation of our study areas ranged from 2700 to 2950 m. Tree-kill soils are immature High Sierra soils formed from granite, pumice, rhyolite, and obsidian parent materials (McGee and Gerlach, 1998).

2.1.1 Ground measurements

We investigated soil CO$_2$ fluxes within five actively degassing areas on Mammoth Mountain documented by Werner et al. (2014) in 2011 and 2012, which represents a period of relatively high emissions (up to 2000 g m^{-2} d^{-1} of CO$_2$). As described by Werner et al. (2014), fluxes were measured along fixed grid points using the accumulation chamber method (Rahn et al., 1996). In situ measurements were obtained using a West Systems® (Florence, Italy) portable flux meter equipped with a LI-COR820 infrared gas analyser. Based on statistical analysis, Werner et al. (2014) found soil CO$_2$ fluxes measured within areas of volcanic CO$_2$ emissions to be significantly elevated over background areas that were dominated by soil respiration of CO$_2$. Maps of soil CO$_2$ flux were simulated from in situ measurements at 1 m

resolution using a sequential Gaussian simulation algorithm by these authors, and we resampled their data to the Airborne Visible/Infrared Imaging Spectrometer (AVIRIS) resolution (13 m) using nearest neighbour resampling. Conventionally, studies of diffuse soil degassing of CO$_2$ on volcanoes have emphasized an understanding of the modes, locations, geometries, and changes in volcanic flank degassing for purposes of volcanological research, hazard assessment, and monitoring. In many cases, volcanologists have focused on areas associated with sufficient emissions of heat and CO$_2$ for vegetation to have been killed off. In this study however, we focused on vegetated areas where somewhat more mildly enhanced levels of volcanic CO$_2$ emissions into the forest ecosystems might be beneficial for plant growth rather than the reverse. As such, we investigated zones and gradients around tree-kill areas, excluding areas that were barren or contained dead trees by filtering by fractional vegetation cover, where appropriate. The tree-kill areas have local soil conditions that are not representative of the larger ecosystem. In addition, because tree-kill areas on Mammoth Mountain are largely associated with "cold" CO$_2$ emissions, we completely avoided confounding influences of hydrothermal heat or acidic vapour emission on ecosystem response. Indeed, there is no significant H$_2$S nor any SO$_2$ present at soil levels at this site, and CO$_2$ makes up $\sim$ 99 % of the gas by volume; see, for example, data in Werner et al. (2014) and Sorey et al. (1998), and a number of papers on volcanic degassing at Mammoth Mountain (Lewicki 2014, 2012, 2008, 2007, 2006). The remaining 1 % is made up of N$_2$ and O$_2$.

The use of a high spatial-resolution time-averaged (to limit the influence of varying meteorological conditions) map of canopy-level atmospheric CO$_2$ concentration would be most applicable to assess ecosystem response to elevated atmospheric CO$_2$ concentrations. However, such maps are unavailable. We therefore took advantage of the extensive record of soil CO$_2$ fluxes available for Mammoth Mountain. Although the effects of elevated CO$_2$ in the soil may be difficult to de-convolve from elevated CO$_2$ in the atmosphere, we treat their effects uniformly. Implications of this are discussed below.

Although the airborne datasets cover a wider region, only points with associated soil CO$_2$ flux measurements were used to derive our models. The CO$_2$ flux measurements were spatially resampled to match the resolution of the other datasets, which resulted in small estimations with low confidence along the edges. To avoid spurious model fits, edge points with CO$_2$ < 5 g m^{-2} d^{-1} were excluded, where the CO$_2$ range is [0,2000] g m^{-2} d^{-1}. In the remainder of this paper, analysed points with elevated CO$_2$ flux will be referred to as eCO$_2$.

2.1.2 AVIRIS

The AVIRIS Classic instrument acquires data from 400 to 2500 nm in 224 contiguous spectral channels. AVIRIS im-
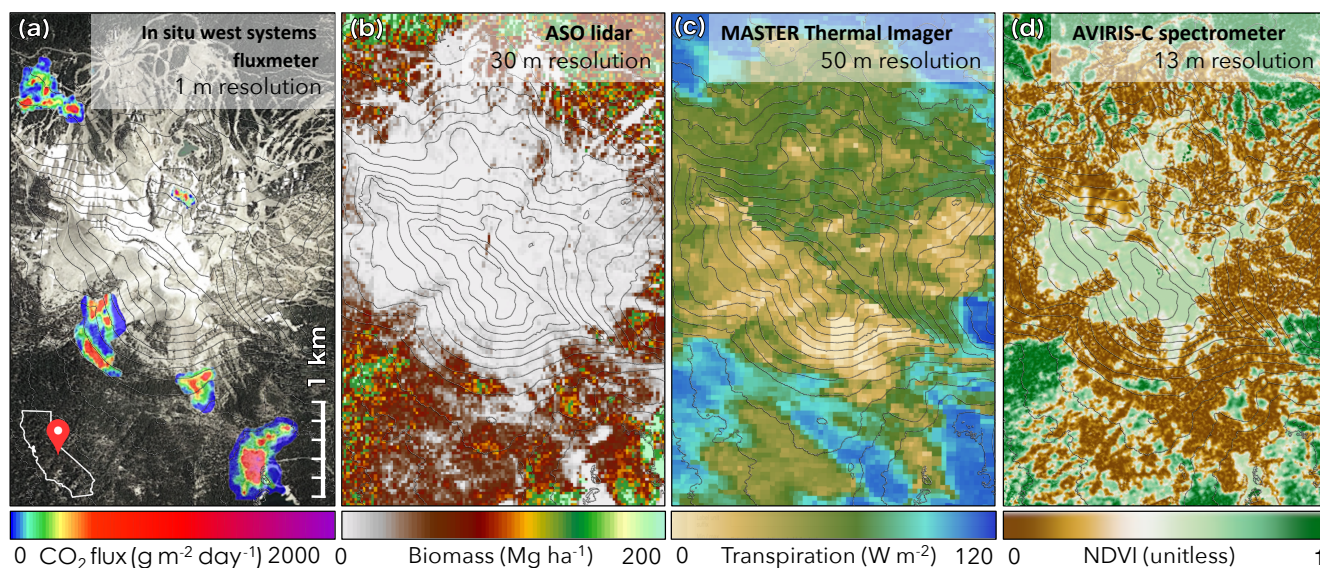
Figure 2. A wealth of remotely sensed imagery has been acquired over Mammoth Mountain. Some data products used in this study include **(a)** maps of soil CO$_2$ flux simulated based on accumulation chamber measurements, shown overlaid on aerial RGB image, **(b)** above-ground biomass derived from the Airborne Snow Observatory (ASO) lidar, **(c)** evapotranspiration derived from the MODIS/ASTER (MASTER) airborne simulator, and **(d)** normalized difference vegetation index (NDVI) derived from the Airborne Visible/Infrared Imaging Spectrometer (AVIRIS image).

agery was acquired over Mammoth in October 2014; this flight was chosen from a number of possible surveys of the area to minimize snow cover and also because of its temporal proximity to the eCO$_2$ ground measurements. The standard level 2 (L2) atmospherically corrected reflectance data (Thompson et al., 2015) were used (available from https://aviris.jpl.nasa.gov/, last access: 19 November 2018), and the data had a spatial resolution of 13 m. These data were collected as part of the NASA HyspIRI Preparatory Airborne Campaign.

Vegetation indices

Vegetation indices are commonly used as an indicator of vegetation health and/or greenness. While many vegetation indices are related, they differ enough to be considered independent variables. For instance, some account for soil moisture, and others weight plant greenness more heavily. This was an exploratory effort in investigating the effects of CO$_2$ on any measure of plant function, composition, and structure, and so we attempted to cover all avenues of investigation. The following indices were derived from the AVIRIS spectral data:

– the normalized difference vegetation index (NDVI)

– simple ratio index

– enhanced vegetation index

– red edge normalized difference vegetation index

– modified red edge simple ratio index

– modified red edge normalized difference vegetation index

– Vogelmann red edge index 1.

Each uses a ratio between narrow bands to represent vegetation health as a single index, and all are described more fully in Thenkabail et al. (2016).

Foliar traits

The chemical composition of plants affects light interactions, especially in the short-wave infrared (Singh et al., 2015). Therefore, imaging spectroscopy can be used to map key vegetation properties, especially those affecting carbon and nutrient interactions. Spectral features, derived from data such as AVIRIS, have been shown to correlate significantly with certain chemicals and plant properties, such as carbon, nitrogen, nitrogen isotope 15, leaf mass per area (LMA), cellulose, and acid-digestible lignin (Singh et al., 2015). These properties are associated with photosynthesis, light-harvesting ability, and nutrient fluxes and can be used to characterize vegetation responses to disturbances or climate trends (Townsend et al., 2008).

The data were first corrected for their bi-directional reflectance distribution function (BRDF), using the Ross-Thick BRDF model with a quadratic volumetric scattering term (Lucht et al., 2000; Roujean et al., 1992). In situ vegetation chemical measurements, along with propagated uncertain-

ties, were used to derive partial least squares regression models for each trait. Since these equations were derived in the nearby area of the Sierra Nevada, these equations were applied to the BRDF-corrected AVIRIS data used in this study.

Infeasible negative numbers were removed for the modelling.

2.1.3 MASTER

The MODIS/ASTER (MASTER) airborne simulator acquires data in 50 channels between 0.4 and 13 μm. We utilized the five thermal channels (10–13 μm), which had been processed to Level 2 (available from https://master.jpl.nasa.gov/, last access: 19 November 2018). MASTER data were acquired in November 2013, with a 50 m spatial resolution.

Land surface temperature

The five thermal bands from MASTER were used to calculate land surface temperature (LST) in a standard Level 2 product. The acquired data were processed to radiance using MODTRAN 5.2 for the atmospheric correction, along with a water vapour scaling method (Tonooka, 2005). The temperature emissivity separation (TES) algorithm was then used to derive LST and spectral emissivity (Gillespie et al., 1998).

The MASTER data are at coarser spatial resolution (50 m) compared to the other datasets (e.g. the working resolution for reprojection is the AVIRIS resolution of 13 m). An ideal dataset would have MASTER acquired at 13 m or similar (~ 10 m; i.e. the scale of an individual tree canopy), but in order to build a comparable dataset for this analysis, we used two resampling methods: the standard nearest neighbour resampling and a statistically principled method proposed in Ma et al. (2018). The statistical model proposed by Ma et al. (2018) represented LST as a combination of low-dimensional random effects linked with basis functions and a Gaussian graphical model (also called Gaussian Markov random field). As demonstrated by Ma et al. (2018), this model provides a flexible and computationally efficient way to characterize potentially complex and non-stationary spatial variability. The parameters of the underlying statistical model were fitted to MASTER LST and evapotranspiration (ET) data at 50 m resolution, using maximum likelihood estimation via an expectation-maximization (EM) algorithm. The resampled data at 13 m spatial resolution were then generated via conditional statistical simulation in which we required that when aggregated back to the original coarse resolution, the resampled data matched the original MASTER data exactly.

Evapotranspiration

ET is the key water variable in ecosystem functioning, indicating plant water use and loss (Fisher et al., 2017). In this study, ET was calculated using the Priestley–Taylor model used by the Jet Propulsion Laboratory (PT-JPL) retrieval (Fisher et al., 2008), which partitions ET into canopy transpiration, soil evaporation, and interception evaporation by transforming potential ET (Priestley and Taylor, 1972) into actual ET using ecophysiological constraints. The ECOSTRESS ET retrieval system was used to incorporate MASTER LST as the thermal input (Fisher et al., 2015); additional ancillary data were incorporated from MODIS and Landsat to constrain meteorological and phenological controls on ET (Famiglietti et al., 2018; Verma et al., 2016; Ryu et al., 2011; Kobayashi et al., 2008). The final ET product used here was only the canopy transpiration component (referred to as ET throughout), as our analytical interest lies only in the vegetation response to eCO₂.

2.1.4 ASO

The Airborne Snow Observatory (ASO, http://aso.jpl.nasa.gov, last access: 19 November 2018) is a coupled lidar (Riegl Q1560) and spectrometer (CASI-1500) mounted on a King Air A90 aircraft and was originally developed to monitor snow in the mountains for water resource management (Painter et al., 2016). The Riegl Q1560 is a dual-scanning lidar with two 1064 nm laser sources; each scanner is tilted in the along-track direction by ±8° and the cross-track direction by ±14° for enhanced retrieval of vertical surfaces. On 27 June 2017 ASO surveyed Mammoth Mountain, retrieving comprehensive lidar point cloud data at a mean of 7.8 pt m^{-2} (max. value ~ 60 pt m^{-2}). Riegl RiPROCESS software was then used to (a) extract point cloud data from raw waveforms (RiANALYZE) using the RiMTA Multiple Time Around algorithm and the RLMS Simple Classification Procedure for classification (SCP1), (b) georeference the point cloud (RiWORLD), and c) export the point cloud to LAS 1.2 in UTM projection (RiWORLD).

Digital terrain model

The ASO lidar point cloud data were filtered to remove outliers by applying an elevation filter to eliminate points that exceed ±100 m from a baseline digital terrain model (DTM) that was obtained from the USGS (United States Geological Survey). The ASO data processing chain includes the identification of ground and off-ground points using the multiscale curvature classification algorithm (Evans and Hudak, 2007) and the calculation of a DTM (3 m × 3 m) that corresponds to the bare soil surface as interpolated from the lidar points classified as ground. Any data voids were then filled-in using search windows that were centred on each void pixel.

Slope and aspect

The slope (steepness) and aspect (direction) were derived directly from the DTM with the terrain analysis processing tool provided by QGIS (https://qgis.org/en/site/, last access: 3 December 2018). These geo-algorithms use a first-order derivative estimation to calculate the slope angle for each pixel in

degrees relative to the horizontal plane and the slope exposition in degrees anticlockwise from north.

Aspect was processed to account for circular angles, by considering

$$K1 = \sin(\alpha + (90 - d)) + 1, \tag{1}$$
$$K2 = \cos(d - \alpha) + 1, \tag{2}$$

where α is the aspect derived from the DTM as described above and d is the prevailing wind direction. In the absence of local data, we assumed the prevailing wind direction to be 270° (e.g. Lewicki and Hilley, 2014; Lewicki et al., 2008; Anderson and Farrar, 2001). (Note that the results presented below were not sensitive to this assumption.)

Canopy height and biomass

The above-ground biomass (AGB) map (30 m × 30 m) was calculated by integrating ASO lidar measurements on forest structure and field inventory data into an allometric equation developed by Garcia et al., (2017):

$$AGB = 11.50 \times MCH^{1.20} \times FC^{0.88}, \tag{3}$$

where MCH and FC are lidar-derived maps of mean canopy height and fractional cover, respectively. Equation (3) was calibrated using AGB reference values derived from 69 field inventory plots located in the Stanislaus National Forest and Yosemite National Park, Sierra Nevada, California. To compute the lidar-derived maps, we first normalized the ASO lidar point cloud to calculate the effective height of vegetation by removing the effect of topography using the DTM described here above. Then, we used the normalized point cloud to calculate a canopy height model (CHM; 1 m × 1 m) by selecting the highest lidar point within each grid cell. Finally, the MCH was calculated by averaging the CHM within each 30 m cell, whereas the FC was computed as the ratio of grid cells covered by vegetation (i.e. MCH > 2 m) to the total number of cells. Note that we defined both MCH and FC with a grid cell size of 30 m in order to agree with the size of the field samples (Garcia et al., 2017). We assumed that Eq. (3) was transferable to our study site because the calibration plots are located only 80 km apart and they are both populated by vegetation of the upper montane and subalpine biotic zones.

2.1.5 Compiling the dataset

The data were first processed to create derived products, and then geolocated to the AVIRIS native resolution of 13 m. That is, for each AVIRIS pixel, the other datasets were resampled and reprojected so that every pixel is associated with a vector of remotely sensed and derived values. Datasets with finer resolution (soil CO_2 flux and lidar) were averaged using the nearest neighbour principle. Derived products with coarser resolution (fractional cover, biomass, and evap-

otranspiration) were resampled using nearest neighbour resampling (e.g. the same biomass value may cover multiple AVIRIS pixels). Because its pixels were the largest, ET was also resampled using a statistically based method, described above in Sect. 2.1.3. We note that although the downscaling approach is robust and statistically sound, we acknowledge that our statistical estimates involving ET will include some uncertainty due to spatial resolution.

Once all pixels had been resampled, we had a total of 5520 data points. For certain experiments we found it necessary to threshold by fractional vegetation cover (FC > 0.7; $n = 55$), although the full dataset was used wherever possible.

The dates of acquisition also differed across datasets. The soil CO_2 flux datasets used in this study were measured during a peak in CO_2 emissions (Werner et al., 2014), and this peak in emissions is thought to affect future plant growth. However, we are observing a snapshot of vegetation function within a zone small enough to be influenced by the same meteorological inputs, and our models have accounted for confounding factors such as slope, elevation, and aspect. Therefore, we considered measurements to be relative on a spatial scale, by comparing neighbouring pixels. The topographic confounders and the fractional cover are derived from the lidar data acquired 4 years after the MASTER data; however, we do not expect changes in the terrain during that time period, and tree presence is unlikely to have changed significantly.

2.2 Statistical modelling

The variables assessed included vegetation indices, plant foliar traits, evapotranspiration, canopy height, and biomass. Given this combination of variables, we tested whether changes in $e\mathrm{CO_2}$ were associated with significant changes in vegetation. We performed a series of multiple linear regressions using $e\mathrm{CO_2}$ as a predictor of various vegetation variables; in particular, regression ensembles build collections of linear regression models, utilizing different predictor combinations, including multiplication of predictor variables. To control for confounding variables including elevation, slope, and aspect (which are topographic proxies for temperature, moisture, and light, respectively), we included them as predictors in the model. Then, the regression coefficient estimate for $e\mathrm{CO_2}$ is an estimate of the change in the response variable due to a change in $e\mathrm{CO_2}$, holding all other variables in the model (the confounders) constant. Random forests were investigated and found to produce similar results. For ease of interpretation, we present here the results of the linear regression ensembles.

Fractional vegetation cover (FC; derived from the lidar) was considered a proxy for vegetation presence. The geometric variables elevation, slope, and aspect were also derived from the lidar point cloud, as described above. Figure 3 illustrates the stratified behaviour of NDVI as coloured by the four confounding variables. There is a particularly clear
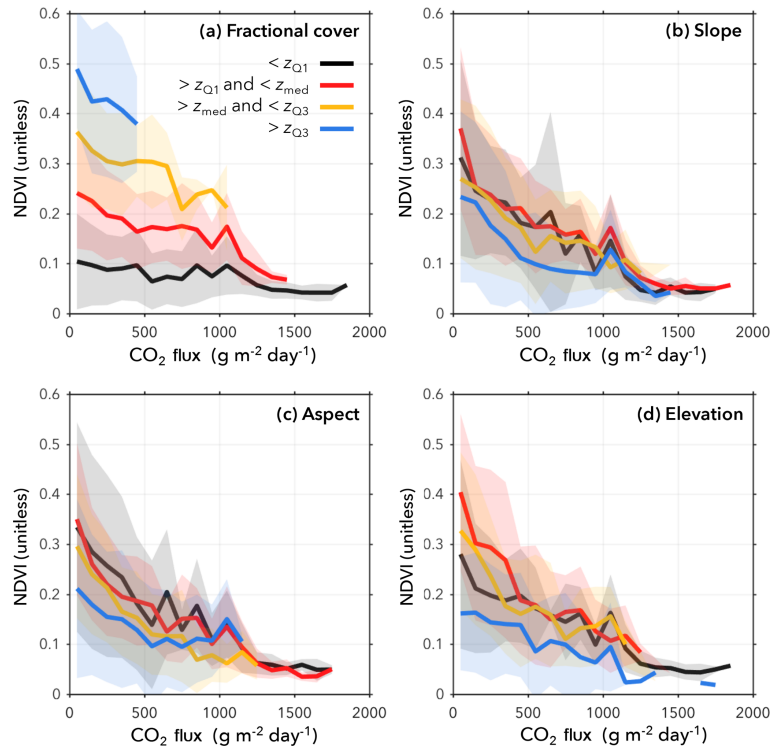
Figure 3. Relationships between many ecological variables, including NDVI, and eCO_2 depend highly on confounding factors. The NDVI data are partitioned into quartiles and coloured such that, if z is the confounding variable (fractional cover, slope, aspect, or elevation), then z_{Q1} is the first quartile of the confounding data; z_{med} is the median of the confounding data; and z_{Q3} is the third quartile. Partitioning by fractional cover yields clear separations in the response variable **(a)** fractional cover, as expected, since rising eCO_2 will have a less measurable effect on sparse vegetation within the pixel. The impact of **(b)** slope, **(c)** elevation, and **(d)** aspect is less clear visually, but their contribution to the model is statistically significant.

separation for fractional cover, which reinforces an expected result: eCO_2 had a negligible effect on vegetation indices and other variables over bare ground but showed higher impacts on fully vegetated pixels. Therefore, we model each vegetation variable, V, as

$$V = b_1 C + b_2 F + b_3 S + b_4 A + b_5 E \quad (4)$$
$$+ f(C, F, S, A, E) + \varepsilon,$$

where C is the elevated soil CO_2 flux, F is the fractional vegetation cover, S is the slope, A is the aspect, E is the elevation, and $\varepsilon \sim N(0, \sigma^2)$ is random error. The function $f(\cdot)$ describes relationships between the predictor variables, which for this model is limited to the first-order interactions:

$$f(C, F, S, A, E) = b_6 C \times F + b_7 C \times S \quad (5)$$
$$+ b_8 C \times A + b_9 C \times E + b_{10} F \times S + \dots.$$

Our hypothesis is $H_A : b_1 \neq 0$; that is, that the effect of eCO_2 on vegetation variable V is different from zero. Our null hypothesis is then $H_0 : b_1 = 0$.

Certain other confounding variables may affect the modelled relationships. The following scenarios and/or variables were also tested as confounders but did not affect the model

outcome: pixel position, site number, and species (plant species were estimated by performing an unsupervised classification on the AVIRIS data). The eCO_2 dataset was also shifted to simulate winds and atmospheric pressure (Ogretim et al., 2013). This did not have an impact on the results.

Additionally, diurnal patterns of mountain slope air flows may dilute and enrich the bulk air mass the trees are exposed to with respect to CO_2 concentrations (Pypker et al., 2007). If these air flow patterns are strong, they may drain the local CO_2 enhancement during morning and evening hours, when these flow events are usually strongest. However, due to the constant nature of these localized enhanced emissions, the gradient, if it was diluted by such effects, re-establishes itself during calmer daytime and night-time hours, as is evident by the volcanically diffuse CO_2 emission signal being detectable from airborne in situ measurements above the investigated sites as well (Gerlach et al., 1999).

When evaluating the dynamics between different variables, it is assumed that the study from which our ground measurements were derived (Werner et al., 2014), covered most of the known CO_2 diffuse emission areas, and so the remainder of the scene exists as a control. The control pixels were also thresholded according to the range of the con-

Table 1. Data sources are shown along with the year in which they were acquired, the original resolution of the dataset, and the method by which they were resampled. All datasets were resampled to the AVIRIS resolution of 13 m.

Data source	Year acquired	Original resolution	Resampling method
Soil CO$_2$ flux	2011–2012	1 m	Nearest neighbour
Canopy height	2017	1 m	Nearest neighbour
Vegetation indices	2014	13 m	Original resolution
Foliar traits	2014	13 m	Original resolution
Fractional cover	2017	30 m	Nearest neighbour
Biomass	2017	30 m	Nearest neighbour
Evapotranspiration	2013	50 m	Nearest neighbour; Ma et al. (2018) resampling

Figure 4. Canopy height is well modelled by the eCO$_2$ model, with an $R^2 = 0.92$ and the 1–1 line shown in black. However, the very tallest trees are not well captured.

founding variables found for the eCO$_2$ points. Therefore, we considered only control points with elevation, slope, and aspect values, respectively, between 2700 and 2950 m, less than 30°, and less than 350°.
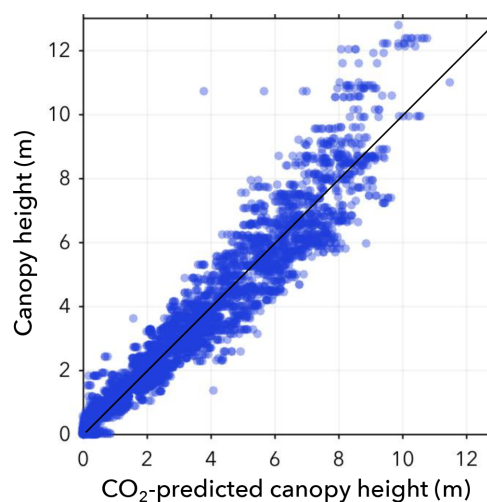
3 Statistical estimation

Although the models were run for 42 explanatory variables (including additional vegetation indices, foliar traits, and other vegetation descriptors), for the sake of brevity we only present the best-performing variables (traits with significant p values are shown, and for all other variables, those with significant p values and $R^2 > 0.5$). For the variables shown in Table 2, the p value of the eCO$_2$ term, b_1, was, for each model, < 0.05 and in most cases $\ll 0.01$. The most significant predictor was determined by ordering terms by p values.

As the confounding variables are expected to drive the behaviour of ecosystem properties, a reduced eCO$_2$ "rank" (in terms of p value significance) does not negate the impact of eCO$_2$ in the models; in fact, each ecosystem variable was strongly influenced by increasing eCO$_2$, given the low p values for the eCO$_2$ coefficient in each model. The rank of each predictor variable is given in Table 3. Since multiplicative terms are allowed, two terms in a single ranking column (say, slope and fractional cover) means that the multiplication between the two terms is the term with the lowest p value. To reduce the complexity of the table, each variable is listed only once, in order of first appearance, whether singly or as a product.
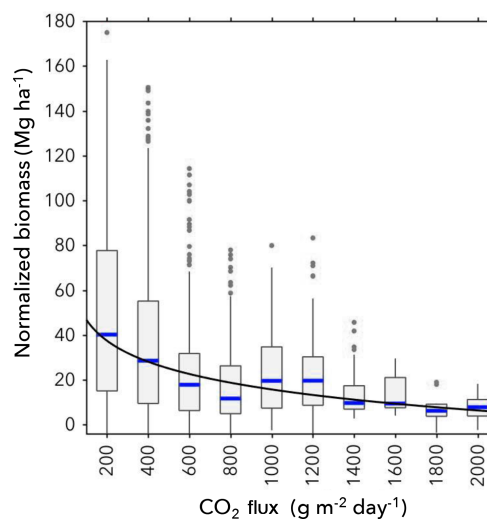
4 Results

4.1 Structure: canopy height and biomass

Canopy height and biomass were accurately modelled with high R^2, as seen in Table 2 and Fig. 4, although eCO$_2$ was the least significant predictor. In each case, eCO$_2$ was still

Figure 5. The biomass model prediction is shown for increasing eCO$_2$. There is high variability at low eCO$_2$ values, but overall there is a small, but apparent, decrease in biomass with increasing eCO$_2$.

regarded as statistically significant but had lower predictive power than the topographic variables.

Figure 5 shows the predictor variable eCO$_2$ against the predicted biomass. There is variability at low eCO$_2$ levels but overall a small decrease in biomass with increasing eCO$_2$. This decrease appears to saturate and is better fit by a logarithmic function; however, given that interactions between terms in the model are allowed, we do not necessarily expect a linear fit, since the eCO$_2$ contribution to the model may be multiplied by other confounding variables. There is also a decrease in biomass variance. In other words, trees exposed to higher eCO$_2$ are more similar.

Table 2. The best-performing vegetation indices (VIs) and traits are shown with the predictive significance of $e\text{CO}_2$ in the model and with their correlation with a regression ensemble that included elevation, slope, aspect, and fractional cover as confounding variables ($n = 5520$). The most significant predictor was determined by ordering terms by p values.

Variable	Most significant predictor term	Estimate for $e\text{CO}_2$ coefficient	Standard error for $e\text{CO}_2$ coefficient	p value for the $e\text{CO}_2$ term	Model R^2
Structure					
Canopy height	Slope, FC	6e−3	1e−3	4e−6	0.92
Biomass	FC	1e−1	2e−2	5e−6	0.83
Composition (vegetation indices)					
Normalized difference vegetation index (NDVI)	$e\text{CO}_2$	−6e−5	8e−6	1e−12	0.68
Red edge normalized difference VI	$e\text{CO}_2$	−3e−5	6e−6	1e−9	0.67
Modified red edge normalized difference VI	$e\text{CO}_2$	−7e−5	6e−6	2e−27	0.65
Vogelmann red edge index 1	$e\text{CO}_2$	−3e−5	1e−5	2e−3	0.64
Enhanced vegetation index	$e\text{CO}_2$	−1e−4	1e−5	2e−22	0.62
Modified red edge simple ratio index	FC	−1e−4	2e−5	5e−10	0.61
Composition (plant foliar traits)					
Trait: canopy nitrogen concentration	Intercept	−8e−3	1e−3	2e−7	0.45
Trait: carbon	FC	3e−2	5e−3	5e−9	0.45
Trait: leaf mass per area (LMA)	Aspect	3e−1	1e−1	6e−2	0.40
Function					
Evapotranspiration (nearest neighbour)	FC	−8e−3	1e−3	5e−16	0.55
Evapotranspiration (statistical resampling)	FC	−3e−4	2e−3	8e−1	0.38

Table 3. The best-performing vegetation indices (VIs) and traits from Table 2 are shown with the ordered significance of every input into the model. Since the model allows multiplication between terms, each input is ordered by first occurrence when ranking p values from smallest (most significant) to largest (least significant).

Variable	Ordered predictor terms (from most to least significant)					
Structure						
Canopy height	Slope, FC	Intercept	Elevation	$e\text{CO}_2$	Aspect	
Biomass	FC	Elevation	Slope	Intercept	$e\text{CO}_2$	Aspect
Composition (vegetation indices)						
Normalized difference vegetation index (NDVI)	$e\text{CO}_2$	FC	Slope	Aspect	Elevation	Intercept
Red edge normalized difference VI	$e\text{CO}_2$, FC	Aspect	Slope	Intercept	Elevation	
Modified red edge normalized difference VI	$e\text{CO}_2$	FC, elevation	Intercept	Aspect	Slope	
Vogelmann red edge index 1	$e\text{CO}_2$, FC	Intercept	Aspect	Elevation	Slope	
Enhanced vegetation index	$e\text{CO}_2$	Intercept	Slope	Elevation, FC	Aspect	
Modified red edge simple ratio index	FC	$e\text{CO}_2$	Intercept	Slope	Aspect	Elevation
Composition (plant foliar traits)						
Trait: canopy nitrogen concentration	Intercept	$e\text{CO}_2$, elevation	FC	Slope, aspect		
Trait: carbon	FC	Elevation	$e\text{CO}_2$	Intercept	Slope	Aspect
Trait: leaf mass per area (LMA)	Elevation	FC	Intercept	$e\text{CO}_2$, slope	Aspect	
Function						
Evapotranspiration (nearest neighbour)	FC	$e\text{CO}_2$	Elevation	Slope	Aspect	Intercept
Evapotranspiration (statistical resampling)	FC	Elevation	Slope	$e\text{CO}_2$	Aspect	Intercept

4.2 Composition: vegetation indices and foliar traits

The performance of different vegetation indices and foliar traits varied. NDVI was best modelled ($R^2 = 0.68$), with eCO_2 as the most significant predictor (p value of 1×10^{-12}). In general, the indices were better modelled than the traits.

Figure 6 shows the predicted model for NDVI (a) and the canopy nitrogen concentration trait (b) against the eCO_2 predictor variable. Modelled NDVI decreases with increasing eCO_2, and there is a decrease in variance with increasing eCO_2. The modelled canopy nitrogen concentration trait increases with increasing eCO_2.

4.3 Function: evapotranspiration

Canopy transpiration was relatively well represented by the eCO_2 model with an $R^2 = 0.55$. For comparison, total ET was not well represented by the eCO_2 model ($R^2 = 0.23$), which is sensible, as eCO_2 is expected to affect only plant transpiration and not soil evaporation. eCO_2 was the second most significant predictor, with fractional vegetation cover the most significant. Given that MASTER data were originally acquired at a much coarser resolution (50 m) than the eCO_2 ground data (1 m) and that both were resampled to 13 m resolution for a spatially consistent analysis, there may have been error introduced due to the resampling. This effect is seen by the much lower model fit with the statistical resampling, although the predicted models follow the same trend. In the remainder of the paper, references to ET refer to the data resampled using nearest neighbour resampling.

Figure 7 shows the ET predicted by the model for the predictor variable eCO_2. There is a decrease in ET for increasing eCO_2, along with a decrease in variance.

4.4 Ecosystem synergies

Given that many of the vegetation indices and traits are only appropriate in the presence of vegetation, a fractional cover threshold of 0.7 was used for the eCO_2 sample, for the sake of evaluating the dynamics between modelled variables. With this threshold, only 55 data points remained, and so the sample size is too small to make claims of statistical significance. Therefore, we present the following results as interesting observations that may inform future data acquisition.

Figure 8 shows the dynamics between variables in the entire scene (i.e. non-elevated, background soil CO_2) versus the points with eCO_2 measurements. It is important to note that in each sub-figure, independent data sources are used to avoid showing intrinsically correlated datasets. Fractional cover and biomass are derived from the ASO lidar data; the vegetation trait data and foliar traits are derived from AVIRIS imagery; and ET is derived from MASTER data. In this case, the variables shown are directly as observed (or derived directly from the data source).

We observed interesting dynamics between ecosystem variables, suggesting great potential for future research. In the eCO_2 subset, NDVI was, on average, lower than that observed for the same fractional cover in the control dataset (Fig. 8a). This is consistent with the model illustration of decreased greenness for increasing eCO_2. Similarly, ET was lower in the eCO_2 subset for pixels with the same NDVI observed in the control, showing a greater degree of stress even when plants have the same greenness (Fig. 8b). In addition, the strong linear relationship between ET and NDVI appears to break down for the points affected by eCO_2.

Canopy nitrogen in the eCO_2 subset increased with fractional cover, unlike the control, which remained flat, which again mimics the modelled data findings (Fig. 8c). ET was lower in the eCO_2 subset for the same biomass, which implies that plants are doubly affected by the enhanced CO_2 – the biomass decreases with increasing eCO_2, and the ET decreases further with decreasing biomass (Fig. 8d). Again, the strong linear relationship between ET and biomass breaks down for those points affected by eCO_2. These findings suggest complex relationships between ecosystem parameters in their response to increasing eCO_2.

5 Discussion

Using airborne remotely sensed ecosystem properties against a ground-measured database of eCO_2 (volcanic excess CO_2 emanating into the forest canopy through the soil), we evaluated the effects of increasing eCO_2 on plant structure, function, and composition. Our aims were to (i) evaluate whether a passively degassing volcanic system is a viable means to study properties of ecosystems, (ii) determine if ecosystem variables are adequately detected using airborne data, and (iii) present key lessons learnt that can enable similar studies over different biomes.

This study has provided initial observations of ecological responses to eCO_2 that are measurable from airborne data. We found that (a) eCO_2 was a significant predictor in regression ensemble models of ecosystem variables and (b) there were visual differences between the sites of increased eCO_2 and the background image. This work also demonstrates that an active volcanic system is a viable way in which to study the CO_2 effect on ecosystems.

The regression ensemble model showed that eCO_2 was a significant predictor for two structural variables (canopy height and biomass), nine composition variables (six vegetation indices, three foliar traits), and a function variable (ET). Therefore, as hypothesized, eCO_2 affects ecosystems in structure, composition, and function, all of which are detectable both with airborne observations as well as within a volcanically derived eCO_2 system. Further evaluation of the model showed that both canopy height and biomass decreased with increasing eCO_2; the vegetation indices decrease with increasing eCO_2; canopy nitrogen concentration
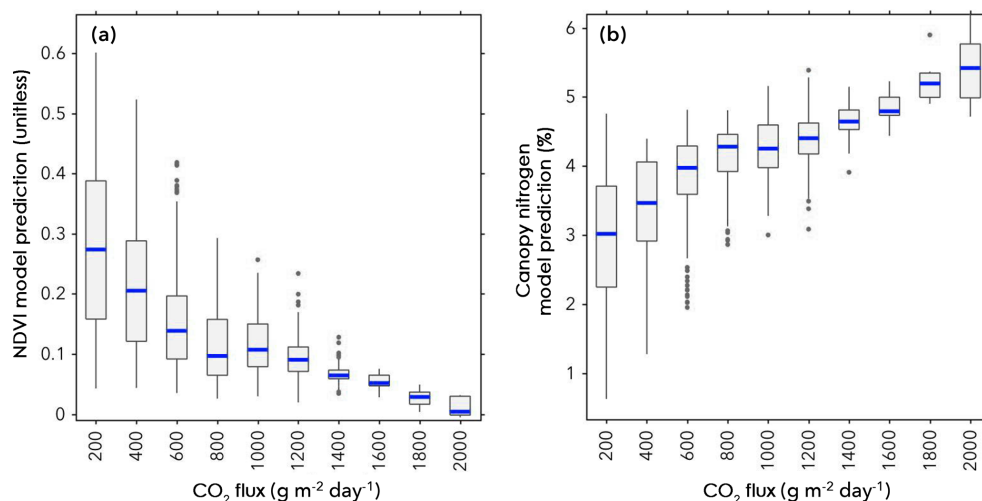
Figure 6. (a) The modelled NDVI prediction is shown for predictor variable eCO_2. There is a decrease in NDVI for increasing eCO_2, despite larger variance at low eCO_2 values. **(b)** The modelled canopy nitrogen concentration trait prediction is shown for predictor variable eCO_2. There is a clear increase in canopy nitrogen concentration with increasing eCO_2.
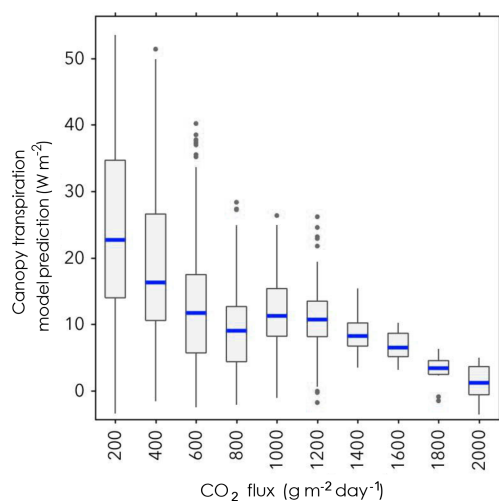
Figure 7. The normalized canopy transpiration prediction is shown against predictor variable eCO_2, for training data with nearest neighbour resampling. There is a clear decrease in ET for increasing eCO_2, with larger variance at low eCO_2 values.

increases; LMA decreases; carbon decreases; and ET decreases.

Some of these observations contrasted with results found in other published studies, while others agreed. For instance, our study found a decrease in NDVI with increasing eCO_2, which correlates to the multispectral satellite findings of Rouse et al. (2010) and Cholathat et al. (2011). In some cases, the decrease others have found can be explained by the tree-kill effect, where vegetation is removed. However, by accounting for fractional cover in our models, we have shown that NDVI decreases independently of fractional cover (see

in Fig. 8). This shows that, regardless of whether the number of trees changes, the greenness of individual trees is reduced. This finding is in direct contrast with the CO_2 fertilization hypothesis, which states that rising CO_2 has a positive effect on plant growth and productivity due to increased availability of carbon, which has been shown using field data (Zhu et al., 2016; Huang et al., 2007). However, this decrease in NDVI could also be explained by a reduction in leaves, rather than a reduction in leaf health, due to more efficient leaves (e.g. higher nutrient concentration, more efficient in water use).

The decrease in canopy height and biomass agrees with the tree-ring study done by Biondi and Fessenden (1999), which also found slower lodgepole pine growth rates in high CO_2 emission areas on Mammoth Mountain. However, a study by Smith et al. (2013) found an increase in biomass in the mixed-species temperate forest FACE experiment. In that experiment, there was large variation between and within species, and the experiment was limited to 4 years. Perhaps a long-term species composition shift due to eCO_2 was the cause of the change in biomass in our study, but we do not have individual tree species-level data to support this hypothesis.

Our model showed an increase in canopy nitrogen, which could indicate species selection or individual plant optimization, given the decrease in NDVI, biomass, and ET. Canopy nitrogen is associated with a plant's investment in photosynthesis (Singh et al., 2015). We also found an increase in canopy nitrogen relative to fractional cover, showing that the change in nitrogen was not impacted by an increase in overall vegetation for those sites (Fig. 8). Tercek et al. (2008) noted that *Dichanthelium lanuginosum* (hot springs panic grass) in Yellowstone had made physiological adjustments to photosynthetic enzymes in response to long-term exposure to CO_2,

and a study of ice cores showed a 40 % decrease in stomatal density over the last 200 years, which parallelled an increase in global CO_2 (Woodward, 1987). However, Sharma and Williams (2009) evaluated vegetation naturally exposed to CO_2 in Yellowstone National Park and found reduced nitrogen at a leaf level in *Pinus contorta* (lodgepole pine) and increased nitrogen at a leaf level for *Linaria dalmatica* (Dalmation toadflax; an invasive, non-native herb). Once again, the species-level differences highlight the need for remote-sensing analysis over areas that encompass wide species variation, in order to understand overall trends.

Kimball et al. (1998) found a slight increase in ET in a FACE experiment over cotton fields, but that increase was within the error of the ET estimation and so was not deemed statistically significant. In contrast, Nendel et al. (2009) found a decrease in ET and an increase in dry above-ground biomass over a FACE crop rotation experiment. In this study, we found a decrease in ET. In addition, we found a decrease in ET relative to both NDVI and biomass, when comparing the points affected by eCO_2 to those unaffected points in the surrounding area. The unaffected sites showed a positive linear relationship between ET and both NDVI and biomass, which appeared to break down for points affected by eCO_2 in both relationships.

The combination of lower NDVI, higher canopy nitrogen, and higher ET suggests a canopy that uses less water with rising CO_2 resulting in higher water use efficiency, with a nutrient-rich canopy. Since leaves are stronger and more efficient, fewer are required for photosynthesis. While biomass increased slightly, the more obvious change was the decrease in the variance of biomass, which points to alignment to more similar trees with elevated CO_2.

High fluxes of CO_2 through soils in kill zones on Mammoth Mountain have likely impacted forest ecosystems through oxygen deprivation in soil pore space, inhibition of root respiration, and soil acidification (McGee and Gerlach, 1998; Farrar et al., 1995; Qi et al., 1994). Since we used soil CO_2 flux as the predictor variable in the model, some of the observed ecosystem responses may therefore be due to the effects of high concentrations of CO_2 on the soil environment or some combination of soil and atmospheric effects. However, by using fractional cover as an input to the model and excluding the kill zones altogether to derive Figure 8, we are focusing on the CO_2 gradient over vegetated areas around these zones, that are unlikely to be affected by soil acidification. The Mammoth Mountain soil CO_2 flux dataset does, however, provide a record of CO_2 emissions that is more stable in space and time than measurements of atmospheric CO_2 concentrations. In particular, forest canopies will through time be exposed to eCO_2 at highly variable levels because the originally mostly invariant eCO_2 once emitted through the soil into the sub-canopy atmosphere is subject to highly variable dispersion from thermal and wind disturbances at minute, diurnal, and seasonal scales (Staebler and Fitzjarrald, 2004). In-canopy concentration measurements of eCO_2

will therefore be highly variable, and, especially if conducted instantaneously, may not be representative of the long-term relative exposure strength in the canopy.

Vegetation at this site is also responding to the partial pressure of CO_2 in the atmosphere, among other gases. A response above the asymptote of the net photosynthetic rate versus internal CO_2 partial pressure (A-Ci curve) would result in very little vegetation response to the partial pressures (Tissue et al., 1999). However, the partial pressures even at elevated molar concentration at Mammoth are about 60 % of those at sea level. The fact that we see systematic ecosystem effects suggests that elevation is not on the flat part of the A-Ci curve. In other words, even if elevation were to reduce the CO_2 effect, we still are seeing strong CO_2 effects regardless, highlighting just how important and strong of a response we are able to detect.

We will clarify that the effects should not necessarily be given a subjective description of "negative"; rather, it is important to note that the CO_2 fertilization effect is unlikely to continue indefinitely, particularly at the same rates that FACE studies have shown only in the short term. All other experiments have been unable to show long-term effects. Our study suggests that over the scale of decades, some of these hypothesized greening or biomass increases may not be sustainable. Other results, such as an increase in canopy nitrogen with increasing CO_2, do seem to remain consistent with our study, however.

This exploratory study leveraged existing data acquired over Mammoth Mountain. We used ASO lidar, AVIRIS, and MASTER data to derive products that describe ecosystem structure, composition, and function and used field eCO_2 measurements to show that elevated CO_2 was a significant predictor of ecosystem variables, including vegetation indices, plant foliar traits, biomass, and evapotranspiration. While our study has shown the promise of airborne remote sensing in detecting measurable ecosystem changes in forest ecosystems on and around a CO_2-emitting volcanic system, it was also completed using an existing ad hoc collection of data. The nature of the collection of data sources enabled us to understand the details of the data characteristics necessary for future studies.

While this study is useful for showing the benefit of both a passively emitting volcanic system and airborne data for evaluating the ecosystem response to eCO_2, we anticipate that more meaningful results would be obtained with all datasets acquired simultaneously, at the same resolution. ET in particular varies over short time periods due to the influence of meteorological inputs, and so multi-temporal acquisitions would provide a better overview of the ecosystem function. Other possible factors could affect this very complex system, some of which have been discussed previously, including pH, oxidative stress, water/nutrient availability, extreme climate events, and plant vigour. More fieldwork and test sites would be needed to rule out many of these factors. Other data, such as photosynthesis, may also add to future

analysis. We note that this study was exploratory and that this study was intended to identify both potential signals as well as design elements for further study.

6 Conclusions

This exploratory study used airborne remote-sensing data, coupled with ground measurements of volcanic soil CO$_2$ flux on a forested volcano, to derive relationships between rising CO$_2$ emissions and ecosystem structure, function, and composition metrics. We have shown that passively emitting volcanic systems are viable environments in which to study CO$_2$ impacts on ecosystems, with eCO$_2$ the most significant predictor in regression ensemble models of several ecological variables, including NDVI, canopy nitrogen concentration, ET, and biomass. When comparing differences between vegetation parameters affected by eCO$_2$ and those estimated over the background scene, we found contrasting patterns and dynamics between ecological variables, showing that a combination of different remote-sensing platforms is capable of providing a comprehensive view of ecosystem responses to long-term elevated volcanic CO$_2$.

Key lessons learnt from this study include the following:

1. Future campaigns should acquire all data at the same or similar resolution at individual tree scale.

2. Significantly more than 55 vegetated tree points are necessary in order to draw meaningful conclusions regarding the dynamics between variables at Mammoth Mountain (which has one dominant tree species). The number of required points in other environments will vary according to ecosystem complexity and will likely far exceed this number.

3. Combining lidar and spectral data across a range of wavelengths yielded a more complete view than using any one data source alone.

References

Anderson, D. E. and Farrar, C. D.: Eddy covariance measurement of CO$_2$ flux to the atmosphere from an area of high volcanogenic emissions, Mammoth Mountain, California, Chem. Geol., 177, 31–42, 2001.

AVIRIS Data Portal: Jet Propulsion Laboratory, California Institute of Technology, available at: https://aviris.jpl.nasa.gov/alt_locator/, last access: 13 December 2018.

Biondi, F. and Fessenden, J. E.: Response of Lodgepole Pine growth to CO$_2$ degassing at Mammoth Mountain, California, Ecology, 80, 2420–2426, 1999.

Boudoire, G., Di Muro, A., Liuzzo, M., Ferrazzini, V., Peltier, A., Gurrieri, S., Michon, L., Giudice, G., Kowalski, P., and Boissier, P.: New perspectives on volcano monitoring in a tropical environment: Continuous measurements of soil CO$_2$ flux at Piton de la Réunion Island, France), Geophys. Res. Lett., 44, 8244–8253, 2017.

Camarda, M., De Gregorio, S., and Gurrieri, S.: Magma-ascent processes during 2005–2009 at Mt. Etna inferred by soil CO$_2$ emissions in peripheral areas of the volcano, Chem. Geol., 330, 218–227, 2012.

Cardellini, C., Chiodini, G., and Frondini, F.: Application of stochastic simulation to CO$_2$ flux from soil: mapping and quantification of gas release, J. Geophys. Res., 108, 2425, https://doi.org/10.1029/2002JB002165, 2013.

Cholathat, R., Li, X., and Ge, L.: Monitoring natural analog of geologic carbon sequestration using multi-temporal Landsat TM images in Mammoth Mountain, Long Valley Cadera, California, Int. Geosci. Remote Se., Vancouver, 24–29 July 2011, 2011.

Cook, A. C., Hainsworth, L. J., Sorey, M. L., Evans, W. C., and Southon, J. R.: Radiocarbon studies of plant leaves and tree rings from Mammoth Mountain, CA: a long-term record of magmatic CO$_2$ release, Chem. Geol., 177, 117–131, 2001.

Drake, B. G., Gonzàlez-Meler, M. A., and Long, S. P.: More Efficient Plants: A Consequence of Rising Atmospheric CO$_2$?, Annu. Rev. Plant Phys., 48, 609–639, https://doi.org/10.1146/annurev.arplant.48.1.609, 1997.

Evans, J. S. and Hudak, A. T.: A multiscale curvature algorithm for classifying discrete return LiDAR in forested environments, IEEE T. Geosci. Remote, 45, 1029–1038, https://doi.org/10.1109/TGRS.2006.890412, 2007.

Farrar, C. D., Sorey, M. L., Evans, W. C., Howle, J. F., Kerr, B. D., Kennedy, B. M., and Southon, J. R.: Forest-killing diffuse CO$_2$ emission at Mammoth Mountain as a sign of magmatic unrest, Nature, 376, 675–678, https://doi.org/10.1038/376675a0, 1995.

Fisher, J. B., and ECOSTRESS Algorithm Development Team: ECOsystem Spaceborne Thermal Radiometer Experiment on Space Station (ECOSTRESS): Level-3 Evapotranspiration Algorithm Theoretical Basis Document, 24 pp, Jet Propulsion Laboratory, Pasadena, 2015.

Fisher, J. B., Melton, F., Middleton, E., Hain, C., Anderson, M., Allen, R., McCabe, M. F., Hook, Baldocchi, D., Townsend, P. A., Kilic, A., Tu, K., Miralles, D. D., Perret, J., Lagouarde, J.-P., Waliser, D., Purdy, A. J., French, A., Schimel, D., Famiglietti, J. S., Stephens, G., and Wood, E. F.: The Future of Evapotranspiration: Global requirements for ecosystem functioning, carbon and climate feedbacks, agricultural management, and water resources, Water Resour. Res., 53, 2618–2626, 2017.

Fisher, J. B., Tu, K., Baldocchi, D. D.: Global estimates of the land-atmosphere water flux based on monthly AVHRR and ISLSCP-II data, validated at 16 FLUXNET sites, Remote Sens. Environ., 112, 901–919, 2008.

Friedlingstein, P., Meinshausen, M., Arora, V. K., Jones, C. D., Anav, A., Liddicoat, S. K., and Knutti, R.: Uncertainties in CMIP5 Climate Projections due to Carbon Cycle Feedbacks, J. Climate, 27, 512–526, 2014.

Garcia, M., Saatchi, S., Ferraz, A., Silva, C.A., Ustin, S., Koltunov, A., and Balzter, H.: Impact of data model and point density on aboveground forest biomass estimation from airborne LiDAR, Carbon Balance and Management, 12, 4, https://doi.org/10.1186/s13021-017-0073-1, 2017.

Gerlach, T. M.: Present-day CO_2 emissions from volcanos, Eos Trans. AGU, 72, 249–255, https://doi.org/10.1029/90EO10192, 1991.

Gerlach, T. M., Doukas, M. P., McGee, K. A., and Kessler, R.: Airborne detection of diffuse carbon dioxide emissions at Mammoth Mountain, California, Geophys. Res. Lett., 26, 3661–3664, 1999.

Giammanco, S., Sims, K. W. W., and Neri, M.: Measurements of ^{220}Rn and ^{222}Rn and CO_2 emissions in soil and fumarole gases on Mt. Etna volcano (Italy): Implications for gas transport and shallow ground fracture, Geochem. Geophy. Geosy., 8, 10, https://doi.org/10.1029/2007GC001644, 2007.

Gillespie, A., Rokugawa, S., Matsunaga, T., Cothern, J. S., Hook, S. J., and Kahle, A. B.: A temperature and emissivity separation algorithm for Advanced Spaceborne Thermal Emission and Relection Radiometer (ASTER) images, IEEE T. Geosci. Remote Sens., 36, 1113–1126, 1998.

Hernández, P. A., Pérez, N. M., Salazar, J. M., Nakai, S., Notsu, K., and Wakita, H.: Diffuse emission of carbon dioxide, methane, and helium-3 from Teide Volcano, Tenerife, Canary Islands, Geophys. Res. Lett., 25, 3311–3314, https://doi.org/10.1029/98GL02561, 1998.

Huang, J.-G., Bergeron, Y., Denneler, B., Berninger, F., and Tardif, J.: Response of forest trees to increased atmospheric CO_2, Crit. Rev. Plant Sci., 26, 265–283, https://doi.org/10.1080/07352680701626978, 2007.

Kerrick, D. M.: Present and past nonanthropogenic CO_2 degassing from the solid earth, Rev. Geophys., 39, 565–585. https://doi.org/10.1029/2001RG000105, 2001.

Kimball, B. A, LaMorte, R. L., Seay, R. S., Pinter Jr, P. J., Rokey, R. R., Hunsaker, D. J., Dugas, W. A., Heuer, M. L., Mauney, J. R., Hendrey, G. R., Lewin, K. F., and Nagy, J.: Effects of free-air CO_2 enrichment on energy balance and evapotranspiration of cotton, Agr. Forest Meteorol., 70, 259–278, 1998.

Kobayashi, H. and Iwabuchi, H.: A coupled 1-D atmosphere and 3-D canopy radiative transfer model for canopy reflectance, light environment, and photosynthesis simulation in a heterogeneous landscape, Remote Sens. Environ., 112, 173–185, 2008.

Kolby Smith, W., Reed, S. C., Cleveland, C. C., Ballantyne, A. P., Anderegg, W. R. L., Wieder, W. R., and Running, S. W.: Large divergence of satellite and Earth system model estimates of global terrestrial CO_2 fertilization, Nat. Clim. Change, 6, 306–310, https://doi.org/10.1038/nclimate2879, 2015.

Körner, C.: Plant CO_2 responses: an issue of definition, time and resource supply, New Phytol., 172, 393–411, https://doi.org/10.1111/j.1469-8137.2006.01886.x, 2006.

Le Quéré, C., Andrew, R. M., Canadell, J. G., Sitch, S., Korsbakken, J. I., Peters, G. P., Manning, A. C., Boden, T. A., Tans, P. P., Houghton, R. A., Keeling, R. F., Alin, S., Andrews, O. D., Anthoni, P., Barbero, L., Bopp, L., Chevallier, F., Chini, L. P., Ciais, P., Currie, K., Delire, C., Doney, S. C., Friedlingstein, P., Gkritzalis, T., Harris, I., Hauck, J., Haverd, V., Hoppema, M., Klein Goldewijk, K., Jain, A. K., Kato, E., Körtzinger, A., Landschützer, P., Lefèvre, N., Lenton, A., Lienert, S., Lombardozzi, D., Melton, J. R., Metzl, N., Millero, F., Monteiro, P. M. S., Munro, D. R., Nabel, J. E. M. S., Nakaoka, S.-I., O'Brien, K., Olsen, A., Omar, A. M., Ono, T., Pierrot, D., Poulter, B., Rödenbeck, C., Salisbury, J., Schuster, U., Schwinger, J., Séférian, R., Skjelvan, I., Stocker, B. D., Sutton, A. J., Takahashi, T., Tian, H., Tilbrook, B., van der Laan-Luijkx, I. T., van der Werf, G. R., Viovy, N., Walker, A. P., Wiltshire, A. J., and Zaehle, S.: Global Carbon Budget 2016, Earth Syst. Sci. Data, 8, 605–649, https://doi.org/10.5194/essd-8-605-2016, 2016.

Lewicki, J. L., Hilley, G. E., Tosha, T., Aoyagi, R., Yamamoto, K., and Benson, S. M.: Dynamic coupling of volcanic CO_2 flow and wind at the HorseshoeLake tree kill, Mammoth Mountain, CA, Geophys. Res. Lett., 34, L03401, https://doi.org/10.1029/2006GL028848, 2006.

Lewicki, J. L., Hilley, G. E., Tosha, T., Aoyagi, R., Yamamoto, K., and Benson, S. M.: Dynamic coupling of volcanic CO_2 flow and wind at the Horseshoe Lake tree kill, Mammoth Mountain, California, Geophys. Res. Lett., 34, L03401, https://doi.org/10.1029/2006GL028848, 2007.

Lewicki, J. L., Fischer, M. L., and Hilley, G. E.: Six-week time series of eddy covariance CO_2 flux at Mammoth Mountain, California: performance evaluation and role of meteorological forcing, J. Volcanol. Geoth. Res., 171, 178–190, https://doi.org/10.1016/j.jvolgeores.2007.11.029, 2008.

Lewicki, J. L., Hilley, G. E., Dobeck, L., and Marino, B. D.: Eddy covariance imaging of diffuse volcanic CO_2 emissions at Mammoth Mountain, CA, USA, Bull. Volcanol., 74, 135–141, 2012.

Lewicki, J. L. and Hilley, G. E.: Multi-scale observations of the variability of magmatic CO_2 emissions, Mammoth Mountain, CA, USA, J. Volcanol. Geoth. Res., 284, 1–15, https://doi.org/10.1016/j.jvolgeores.2014.07.011, 2014.

Lewicki, J. L., Hilley, G. E., Shelly, D. R., King, J. C., McGeehin, J. P., and Mangan, M.: Crustal migration of CO_2-rich magmatic fluids recorded by tree-ring radiocarbon and seismicity at Mammoth Mountain, CA, USA, Earth Planet. Sci. Lett., 390, 52–58, 2014.

Lewin, K. F., Hendrey, G. R., Nagy, J., and LaMorte, R. L.: Design and application of a free-air carbon diox-

ide enrichment facility, Agric. Forest Meteorol., 70, 15–29, https://doi.org/10.1016/0168-1923(94)90045-0, 1994.

List, M. R.: Geologic remote sensing and GIS evaluation of volcanogenic CO$_2$-induced tree kills: Mammoth Mountain, California, 1991–2004, M.S. Thesis, CSUS, 2005.

Ma, P., Kang, E. L., Braverman, A., and Nguyen, H.: Spatial statistical downscaling for constructing high-resolution nature runs in global observing system simulation experiments, in review, 2018.

Mason, E., Edmonds, M., and Turchyn, A. V.: Remobilization of crustal carbon may dominate volcanic arc emissions, Science, 357, 290–294, 2017.

MASTER Data Products: Jet Propulsion Laboratory, California Institute of Technology, available at: https://masterprojects.jpl.nasa.gov/L2_Products/, last access: 13 December 2018.

McGee, K. A. and Gerlach, T. M.: Annual cycle of magmatic CO$_2$ in a tree-kill soil at Mammoth Mountain, California: Implications for soil acidification, Geology, 26, 463–466, https://doi.org/10.1130/0091-7613(1998)026<0463:ACOMCI>2.3.CO;2, 1998.

McGuire, A. D., Melillo, J. M., and Joyce, L. A.: The Role of Nitrogen in the Response of Forest Net Primary Production to Elevated Atmospheric Carbon Dioxide, Annu. Rev. Ecol. Syst., 26, 473–503, 1995.

Nendel, C., Kersebaum, K. C., Mirschel, W., Manderscheid, R., Weigel, H.-J., and Wenkel, K.-O.: Testing different CO$_2$ response algorithms against a FACE crop rotation experiment, NJAS – Wageningen, J. Life Sci., 57, 17–25, 2009.

Norby, R. J., De Kauwe, M. G., Domingues, T. F., Duursma, R. A., Ellsworth, D. S., Goll, D. S., and Zaehle, S.: Model–data synthesis for the next generation of forest free-air CO$_2$ enrichment (FACE) experiments, New Phytol., 209, 17–28, https://doi.org/10.1111/nph.13593, 2016.

Ogretim, E., Crandall, D., Gray, D. D., and Bromhai, G. S.: Effects of Atmospheric Dynamics on CO$_2$ Seepage at Mammoth Mountain, California USA, Journal of Computational Multiphase Flows, 5, 283–294, 2013.

Painter, T. H., Berisford, D. F., Boardman, J. W., Bormann, K. J., Deems, J. S., Gehrke, F., Hedrick, A., Joyce, M., Laidlaw, R., Marks, D., Mattmann, C., McGurk, B., Ramirez, P., Richardson, M., Skiles, S. M., Seidel, F. C., and Winstral, A.: The Airborne Snow Observatory: Fusion of scanning lidar, imaging spectrometer, and physically-based modeling for mapping snow water equivalent and snow albedo, Remote Sens. Environ., 184, 139–152. https://doi.org/10.1016/j.rse.2016.06.018, 2016.

Perez, N. M., Hernandez, P. A., Padilla, G., Nolasco, D., Barrancos, J., Melian, G., and Ibarra, M.: Global CO$_2$ emission from volcanic lakes, Geology, 39, 235–238, 2011.

Peterson, B. J. and Melillo, J. M.: The potential storage of carbon caused by eutrophication of the biosphere, Tellus B, 37, 117–127, https://doi.org/10.1111/j.1600-0889.1985.tb00060.x, 1985.

Pickles, W. L., Kasameyer, P. W., Martini, B. A., Potts, D. C., and Silver, E. A.: Geobotanical Remote Sensing for Geothermal Exploration, Geothermal Resources Council 2001 Annual Meeting, San Diego, California, 26–29 August, 2001.

Potter, D. A.: Forested Communities of the Upper Montane in the Central and Southern Sierra Nevada, United States Department of Agriculture General Technical Report PSW-GTR-169, 1998.

Pypker, T. G., Unsworth, M. H., Mix, A. C., Rugh, W., Ocheltree, T., Alstad, K., and Bond, B. J.: Using Nocturnal Cold Air Drainage Flow to Monitor Ecosystem Processes in Complex Terrain, Ecol. Appl., 17, 702–714, 2007.

Qi, J., Marshall, J. D., and Mattson, K. G.: High soil carbon dioxide concentrations inhibit root respiration of Douglas fir, New Phytol., 128, 435–442, 1994.

Rahn, T. A., Fessenden, J. E., and Wahlen, M.: Flux chamber measurements of anomalous CO$_2$ emission from the flanks of Mammoth Mountain, California, Geophys. Res. Lett., 23, 1861–1864, 1996.

RiANALYZE: available at: http://www.riegl.com/products/software-packages/rianalyze/, last access: 8 July 2017.

Rouse, J. H., Shaw, J. A., Lawrence, R. L., Lewicki, J. L., Dobeck, L. M., Repasky, K. S., and Spangler, L. H.: Multi-spectral imaging of vegetation for detecting CO$_2$ leaking from underground, Environ. Earth Sci., 60, 313–323, 2010.

Ryu, Y., Baldocchi, D. D, Kobayashi, H., van Ingen, C., Li, J., Black, T. A., Beringer, J., van Gorsel, E., Knohl, A., Law, B. E., and Roupsard, O.: Integration of MODIS land and atmosphere products with a coupled-process model to estimate gross primary productivity and evapotranspiration from 1 km to global scales, Global Biogeochem. Cy., 25, GB4017, https://doi.org/10.1029/2011GB004053, 2011.

Schimel, D. S.: Terrestrial ecosystems and the carbon cycle, Glob. Change Biol., 1, 77–91, https://doi.org/10.1111/j.1365-2486.1995.tb00008.x, 1995.

Schimel, D., Stephens, B. B., and Fisher, J. B.: Effect of increasing CO$_2$ on the terrestrial carbon cycle, P. Natl. Acad. Sci. USA, 112, 436–441. https://doi.org/10.1073/pnas.1407302112, 2015.

Schwandner, F. M., Gunson, M. R., Miller, C. E., Carn, S. A., Eldering, A., Krings, T., and Podolske, J. R.: Spaceborne detection of localized carbon dioxide sources, Science, 358, eaam5782, https://doi.org/10.1126/science.aam5782, 2017.

Schwandner, F. M., Seward, T. M., Gize, A. P., Hall, P. A., and Dietrich, V. J.: Diffuse emission of organic trace gases from the flank and crater of a quiescent active volcano (Vulcano, Aeolian Islands, Italy), J. Geophys. Res.-Atmos., 109, D04301, https://doi.org/10.1029/2003JD003890, 2004.

Sharma, S. and Williams, D. G.: Carbon and oxygen isotope analysis of leaf biomass reveals contrasting photosynthetic responses to elevated CO$_2$ near geologic vents in Yellowstone National Park, Biogeosciences, 6, 25–31, https://doi.org/10.5194/bg-6-25-2009, 2009.

Singh, A., Serbin, S. P., McNeil, B. E., Kingdon, C. C., and Townsend, P. A.: Imaging spectroscopy algorithms for mapping canopy foliar chemical and morphological traits and their uncertainties, Ecol. Appl., 25, 2180–2197, 2015.

Smith, A. R., Lukac, M., Hood, R., Healey, J. R., Miglietta, F., and Godbold, D. L.: Elevated CO$_2$ enrichment induces a differential biomass response in a mixed species temperate forest plantation, New Phytol., 198, 156–168, 2013.

Sorey, M. L., Evans, W. C., Kennedy, B. M., Farrar, C. D., Hainsworth, L. J., and Hausback, B.: Carbon dioxide and helium emissions from a reservoir of magmatic gas beneath Mammoth Mountain, California, J. Geophys. Res.-Sol. Ea, 103, 15303–15323, 1998.

Staebler, R. M. and Fitzjarrald, D. R.: Observing subcanopy CO$_2$ advection, Agr. Forest Meteorol., 112, 139–156, 2004.

Tercek, M. T., Al-Niemi, T. S., and Stout, R. G.: High Levels of Carbon Dioxide in YellowStone National Park: A Glimpse into the Future?, Yellowstone Science, 16, 12–19, 2008.

Thenkabail, P. S., Lyon, J. G., and Huete, A.: Hyperspectral Remote Sensing of Vegetation, CRC Press, Taylor and Francis Group, 405–406, 2016.

Thompson, D. R., Gao, B.-C., Green, R. O., Roberts, D. A., Dennison, P. E., and Lundeen, S. R.: Atmospheric correction for global mapping spectroscopy: ATREM advances for the HyspIRI preparatory campaign, Remote Sens. Environ., 167, 64–77, 2015.

Tissue, D. T., Griffin, K. L., and Ball, J. T.: "Photosynthetic Adjustment in Field-Grown Ponderosa Pine Trees after Six Years of Exposure to Elevated CO_2", Tree Physiol., 19, Oxford University Press, 221–228, 1999.

Tonooka, H.: Accurate Atmospheric Correction of ASTER Thermal Infrared Imagery Using the WVS Method, IEEE Trans. Geos. Remote Sens., 43, 2778–2792, 2005.

Verma, M., Fisher, J. B., Mallick, K., Ryu, Y., Kobayashi, H., Guillaume, A., Moore, G., Ramakrishnan, L., Hendrix, V., Wolf, S., Sikka, M., Kiely, G., Wohlfahrt, G., Gielen, B., Roupsard, O., Toscano, P., Arain, M. A., and Cescatti, A.: Global surface net-radiation at 5 km from MODIS Terra, Remote Sens., 8, 1–20, 2016.

Werner, C. and Brantley, S.: CO_2 emissions from the Yellowstone volcanic system, Geochem. Geophy. Geosy., 4, 1061, https://doi.org/10.1029/2002GC000473, 2003.

Werner, C., Bergfeld, D., Farrar, C. D., Doukas, M. P., Kelly, P. J., and Kern, C.: Decadal-scale variability of diffuse CO_2 emissions and seismicity revealed from long-term monitoring (1995–2013) at Mammoth Mountain, California, USA, J. Volcanol. Geotherm. Res., 289, 51–63, https://doi.org/10.1016/j.jvolgeores.2014.10.020, 2014.

Woodward, F. I.: Stomatal numbers are sensitive to increases in CO_2 from pre-industrial levels, Nature, 327, 617–618, 1987.

Zhu, Z., Piao, S., Myneni, R. B., Huang, M., Zeng, Z., Canadell, J. G., Ciais, P., Sitch, P., Friedlingstein, P., Arneth, A., Cao, C., Cheng, L., Kato, E., Koven, C., Li, Y., Lian, X., Liu, Y., Liu, R., Mao, J., Pan, Y., Peng, S., Peñuelas, J., Poulter, B., Pugh, T. A. M., Stocker, B. D., Viovy, N., Wang, X., Wang, Y., Xiao, Z., Yang, H., Zaehle, S., and Zeng, N.: Greening of the Earth and its drivers, Nat. Clim. Change, 6, 791–795, 2016.